Applied Surface Science 735 (2026) 166656

Contents lists available at ScienceDirect

Applied Surface Science

journal homepage: www.elsevier.com/locate/apsusc

Full Length Article

Plasma-induced durable superhydrophilic polypropylene nonwovens for enhanced oil/water separation

Xueqing Zhao [a,b,1], Changying Chen [b,c,1], Guanshui Ma [b,*], Peng Guo [b], Rende Chen [b], Peiling Ke [b], Aiying Wang [b,d,**]

[a] College of Chemical Engineering, Zhejiang University of Technology, Hangzhou 310032, China
[b] State Key Laboratory of Advanced Marine Materials, Zhejiang Key Laboratory of Extreme-environmental Material Surfaces and Interfaces, Ningbo Institute of Materials Technology and Engineering, Chinese Academy of Sciences, Zhejiang, Ningbo 315201, China
[c] School of Materials Science and Chemical Engineering, Ningbo University, Zhejiang, Ningbo 315211, China
[d] Center of Materials Science and Optoelectronics Engineering, University of Chinese Academy of Sciences, Beijing 100049, China

ARTICLE INFO

Keywords:
Plasma polymerization and treatment
Polypropylene nonwoven fabrics
Surface micro-nano structure
Durablewettability

ABSTRACT

Polypropylene (PP) nonwoven fabrics offer many advantages, such as interconnected microstructures, flexibility, and chemical stability. However, their intrinsic hydrophobicity severely restricts applications in oil–water separation. In this work, inductively coupled plasma-enhanced chemical vapor deposition (IC-PECVD) was employed to endow PP nonwoven fabrics with superhydrophilic-underwater superoleophobic properties. After hexamethyldisiloxane deposition, a subsequent 5 min oxygen plasma treatment transformed the fabric surface from highly hydrophobic (>130°) to superhydrophilic (complete wetting), and from lipophilic (~60.3°) to underwater superoleophobic (~151°). The fiber surface evolved progressively from smooth to conical structure with high roughness and distributed different sizes of nanoparticles, while hydrophilic oxygen-containing polar functional groups were introduced. Importantly, the coating designed by this unique combination improved the crosslinking degree of the fiber surface, stabilized hydrophilic hydroxyl, carboxyl and other functional groups, which greatly improved the problem of plasma aging effect, maintaining high stability in air over 260 days. The long-term stability and cyclic oil–water separation tests were carried out on the pre-wetted modified nonwoven fabrics. The fabrics consistently exhibited an oil–water separation efficiency exceeding 99.0%, along with long-term stability, chemical resistance and self-cleaning capability. These results are broadening the application of modified nonwoven fabrics in the field of actual oil–water separation.

1. Introduction

The escalating global water pollution crisis, exacerbated by oil contaminants, demands urgent technological solutions. Oily wastewater discharge forms impermeable surface films that disrupt essential oxygen exchange between aquatic and atmospheric environments. Synthetic oils are particularly concerning due to their limited biodegradability, which threatens marine ecosystems, human health, and sustainable socioeconomic development through bioaccumulation [1,2]. Inspired by biological prototypes such as fish scales, superhydrophilic surfaces (water contact angle < 5°) are achieved through the synergy of surface roughness engineering and high-energy chemical modifications [3–6]. These bifunctional interfaces integrate superhydrophilicity with underwater superoleophobicity, enabling efficient oil–water separation through selective water permeation while repelling hydrophobic contaminants. This membrane-based approach offers operational simplicity and environmental compatibility compared to conventional separation techniques.

Fabric-based materials have emerged as promising separation media because their interconnected microporous networks facilitate hydraulic transport upon hydrophilic modification. They also offer advantages such as cost-effectiveness, environmental friendliness, and application

* Corresponding author.
** Corresponding author at: State Key Laboratory of Advanced Marine Materials, Zhejiang Key Laboratory of Extreme-environmental Material Surfaces and Interfaces, Ningbo Institute of Materials Technology and Engineering, Chinese Academy of Sciences, Zhejiang, Ningbo 315201, China.
E-mail addresses: maguanshui@nimte.ac.cn (G. Ma), aywang@nimte.ac.cn (A. Wang).
[1] Zhao Xueqing and Chen Changying are co-first authors.

https://doi.org/10.1016/j.apsusc.2026.166656
Received 28 October 2025; Received in revised form 23 December 2025; Accepted 19 March 2026
Available online 19 March 2026
0169-4332/

flexibility [7]. Polypropylene nonwoven fabrics exhibit advantageous mechanical flexibility, chemical inertness, and inherent textile properties, rendering them promising substrate materials for oil–water separation membranes. Nevertheless, their intrinsic hydrophobicity necessitates surface modification for practical implementation. Various methods have been developed to control the surface wettability of practical applications. For example, Yang et al. [8] developed a cotton fabric-based membrane with special wettability and excellent anti-contamination ability by using a chemical etching method. Likewise, Lee et al. [9] obtained a superhydrophilic ramie fabric by using a mild alkali to remove its wax, rough and gummy veneers in the raw ramie fiber, which had a long-term stability of more than 90 days and a robust self-cleaning ability to clean spilled low sulfur fuel oils. Zhang et al. [10] utilized the synergistic self-assembly of chitosan and hydroxylated multi-walled carbon nanotubes on cotton fabric to construct a rough structure, which was combined with hydrophilic modification using polyvinyl alcohol for enhancing the wettability of cotton fabrics. However, these complex and costly preparation methods produced a large amount of waste liquid, which harms the operators and the environment. Beyond these conventional wet-chemical methods, the field of advanced separation materials is rapidly evolving towards designing membranes with exceptional durability and anti-fouling properties [11]. For instance, nature-inspired superwetting membranes have been developed for challenging emulsified oil/water mixtures, while Janus membranes with hydrogel-like coatings exhibit remarkable fouling and wetting resistance in harsh processes like membrane distillation [12,13]. These advancements underscore the critical need for separation media that are not only efficient but also robust and long-lasting [14].

Plasma treatment presents a green alternative through non-equilibrium gas discharges that selectively modify surface properties without bulk alterations [15]. The vacuum-based technique enables atomic-scale precision (1–100 nm surface penetration) for simultaneous etching, functionalization and polymerization [16–18]. For different substrate materials, selecting an appropriate plasma gas source is crucial. It is found that plasma etching with hydrogen, argon and oxygen can improve the hydrophilicity of the substrate surface. Hydrogen and argon plasma mainly occur defluorination reaction, while oxygen plasma mainly occurs dehydrogenation reaction [19]. For polypropylene nonwoven fabrics composed entirely of carbon and hydrogen, the dehydrogenation reaction induced by oxygen plasma treatment and the incorporation of oxygen are extremely effective in improving their hydrophilicity.

However, a major limitation is that the surfaces treated by plasma etching frequently exhibit hydrophobicity recovery and temporal instability, which seriously affects the practical application of materials [20,21]. The research demonstrates that plasma polymerization following plasma etching produces a more stable surface, mitigating time-dependent degradation and enabling sustained hydrophilic modification. Hexamethyldisiloxane (HMDSO) emerges as an optimal precursor for plasma-enhanced chemical vapor deposition (PECVD), combining rapid polymerization kinetics with exceptional thermal stability [22,23]. The HMDSO-derived siloxane matrix undergoes subsequent oxygen plasma treatment, where CH_3 group replacement with hydrophilic moieties (−Si-O-) enhances surface energy. Although numerous studies have reported the fabrication of superhydrophilic surfaces via HMDSO plasma polymerization, detailed insights into the effects of HMDSO on the surface morphology and chemical composition of fabrics remain limited [24–27]. Moreover, the underlying mechanisms of superhydrophilic surface formation and their applications in oil–water separation are still insufficiently explored.

In this work, polypropylene nonwoven fabrics were sequentially modified via oxygen plasma etching, HMDSO deposition, and oxygen plasma treatment to construct membranes with superhydrophilic and underwater superoleophobic properties. The evolution of surface morphology and chemical composition was further analyzed, including the role of treatment time in surface functionalization. Furthermore, the timeliness, self-cleaning capabilities and oil–water separation efficiency were evaluated, and the practical application of modified nonwoven fabrics in the field of oil–water separation was analyzed.

2. Experimental section

2.1. Materials and fabrication of modified nonwoven fabrics

Polypropylene nonwoven fabrics (Zhejiang Kaijie Nonwoven Fabric Co., Ltd.) was used as the experimental substrate. Samples were soaked in acetone for 3 min to remove surface pollutants, then ultrasonically cleaned with deionized water and dried. The inductively coupled plasma-enhanced chemical vapor deposition (ICP-PECVD-13.56 MHz) equipment was utilized to modify the nonwoven fabrics. Specifically, the cleaned and dried samples were mounted on the cathode plate inside the reaction chamber using conductive adhesive. The chamber was sealed and pumped down. High-purity oxygen (99.99%) was introduced when the vacuum was pumped to 3.99×10^{-3} Pa. The gas flow rate was set to 100 mL/min, while the operating voltage remained at 600 V. The working pressure was set to be 27 Pa, and the processing time was 30 min. After etching, the chamber was pumped down again to below 3.99×10^{-3} Pa, and HMDSO was introduced. The deposition was performed under the following conditions: a gas flow rate of 40 mL/min, a working voltage of 600 V, a working pressure of 27 Pa, and a processing time of 20 s. After deposition, the first step was repeated with the activation time adjusted to 1, 2, 3, 4, and 5 min.

2.2. Morphological and compositional characterization

The microstructural morphology of the samples before and after modification was examined using a field-emission scanning electron microscope (SEM, FEI Quanta FEG 250, USA). Particle size distribution was analyzed from SEM images using Image J software. Because the polypropylene nonwoven fabric is non-conductive, samples were sputter-coated with a platinum layer (100 mA, 100 s) prior to imaging. Surface roughness measurements were performed using an atomic force microscope (AFM, Dimension ICON, Bruker, USA). Due to the relatively small diameter and curved surface of the fibers, the scan area was carefully selected to ensure accurate topographic representation, and multiple measurements were taken at different locations to obtain a representative average roughness value. Surface chemical composition was analyzed by microscopic Fourier transform infrared spectroscopy in attenuated total reflectance (ATR) mode (Micro-FTIR, iS 50, Semirfei, USA). Spectra were acquired over the wavenumber range of 400–4000 cm^{-1} with a resolution of 2 cm^{-1}, a wavenumber accuracy of 0.01 cm^{-1}, and 32 scans. Elemental composition and chemical bonding states were determined by X-ray photoelectron spectroscopy (XPS, Axis Ultra DLD, UK). The spectra were calibrated to the C1s peak at 284.8 eV. Peak deconvolution was performed using CasaXPS software with a Shirley background, applying Gaussian–Lorentzian peak shapes (70% Gaussian, 30% Lorentzian) and a full width at half maximum of approximately 1.2 eV.

2.3. Wettability and cyclic oil–water separation for modified nonwoven fabrics

Surface wettability was evaluated with a contact angle goniometer (Data Physics, OCA20, Germany) in static mode using 3.0 μL droplets, with the values averaged from three different positions. Deionized water droplets were used to measure the water contact angle, while poly-α-olefin (PAO) synthetic base oil stained with oil red was employed to measure the underwater oil contact angle.

For the cyclic oil–water separation, the oil–water mixture was obtained by combining 20 mL of dyed PAO oil with 40 mL of deionized water. In the process of oil/water separation, the modified nonwoven fabrics were pre-wetted with water and positioned in the center of the

separation device. The separated water was collected in a conical flask at the bottom. For the aging test, the water contact angle measurements were taken every five days. Chemical stability tests were conducted by immersing the modified samples in acidic, alkaline, and saline solutions (3.5 wt% NaCl) for 24 h. Deionized water was used as the base solution, and the pH values of 1, 5, 9, and 13 were adjusted by adding hydrochloric acid or sodium hydroxide to obtain the corresponding acidic and alkaline media. After immersion, the samples were rinsed with deionized water and dried in an oven at 60°C before water contact angle (WCA) and SEM analysis.

3. Results and discussion

The surface evolution of polypropylene fibers during the multi-step plasma modification process is schematically illustrated in Fig. 1. The surface characteristics of fibers, which are the primary constituents of nonwoven fabrics, directly influences its macroscopic performance of the fabrics. Prior to oxygen treatment, all samples underwent a consistent 30 min oxygen pre-etching and 20 s HMDSO deposition. The surface morphology of the untreated Polypropylene nonwoven fabrics and Polypropylene fabrics with 30 min etching and 20 s deposition were presented in Fig. 2. The untreated polypropylene nonwoven fabrics exhibited a smooth surface with no discernible protrusions, and a roughness of only 1.26 nm (Fig. 2a). After 30 min etching, the fabrics surface displayed a conical protrusion structure, with a roughness of 3.0 nm (Fig. 2b). Following a further 20 s deposition, the fabrics surface preserved a rather full post-etching morphology, with small nanoparticles (4–20 nm) uniformly distributed within surface depressions (Fig. 2c). The consistent pretreatment resulted in no significant difference between the SEM images of the fibers at micrometer scale (Fig. 3a-e). The nanoscale fibers surface covered with conical cluster structures and nanoparticles of different sizes, revealed that the surface morphology became increasingly complex with extended oxygen plasma treatment [28]. Furthermore, the size of the nanoparticles increased, leading to the formation of larger nanospherical agglomerates.

Fig. 3 depicted the surface micro-morphology of Polypropylene fabrics with various treatment time. Polypropylene fibers, a semi-crystalline polymer, exhibited a heterogeneous surface morphology comprising crystalline and amorphous regions. The crystalline domains with ordered and densely packed polymer chains possessed higher bond energies, while the amorphous regions were comparatively less ordered and lower bond energies. Oxygen plasma etching selectively targets the amorphous regions due to their lower crystallinity and weaker bond energies. This differential etching behavior resulted in varying etch rates, which led to the formation of nano-cone structure [29,30]. Nanoparticles formation followed three steps: (i) nucleation of primary particles, (ii) aggregation and condensation, and (iii) surface expansion [31]. The formation of spherical nanoparticles deposited on the fibers surface was related to the breakage of HMDSO monomers upon plasma discharge. With the increase of oxygen plasma treatment time, the morphology became more complex, and the nanoparticle size increased steadily, promoting the aggregation of spherical particles. Oxygen plasma bombardment further promoted HMDSO monomer scission, generating free radicals and increasing nucleation sites, thereby enhancing particle adhesion and growth. Furthermore, the protruding nanocone features on the fiber surface facilitated plasma interaction at these elevated sites, resulting in the preferential deposition and growth of larger nanoparticles at the cone apexes.

Fig. 4a illustrates the variation in water contact angle (WCA) and underwater oil contact angle (UOCA) of polypropylene nonwoven fabrics with varying oxygen plasma treatment time. After 1 min of treatment, the fabric surface exhibited a WCA of ~ 73.3°, confirming its hydrophilic nature. Extending the treatment to 2–5 min led to immediate water penetration, a characteristic of the superhydrophilic state, which was consistent with Wenzel's model [32]. The UOCA was approximately 25.9° after 1 min oxygen plasma treatment, indicating lipophilicity. The UOCA increased to approximately 133°, 136°, 144°, and 151.3° after 2, 3, 4, and 5 min of treatments, respectively. The O_2 plasma treatment for more than 2 min resulted in excellent underwater oleophobicity, and the fabric treated for 5 min achieved an underwater superoleophobic state (UOCA > 150°). Furthermore, the modified fabric (5 min treatment) exhibited underwater oleophobicity against various oils. The variation in UOCA among different oils (Fig. 4b) was primarily attributed to differences in oil viscosity, which confirmed the applicability of the modified fabric in diverse oil–water environments.

The untreated nonwoven fabrics showed hydrophobicity (approximately 133.8°) and underwater lipophilicity (approximately 61°). After HMDSO deposition and subsequent oxygen plasma treatment, the samples became superhydrophilic and underwater superoleophobic. According to the Wenzel equation:

$$\cos\theta_{Wenzel} = r\cos\theta \quad (1)$$

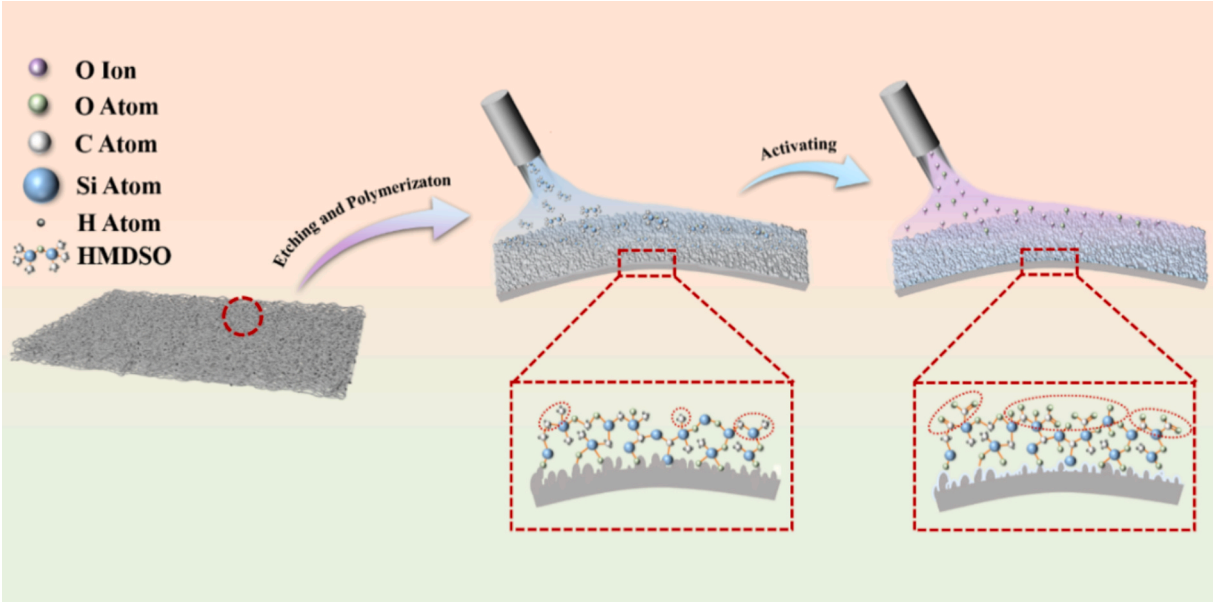

Fig. 1. Schematic illustration of surface evolution during the multi-step plasma modification.

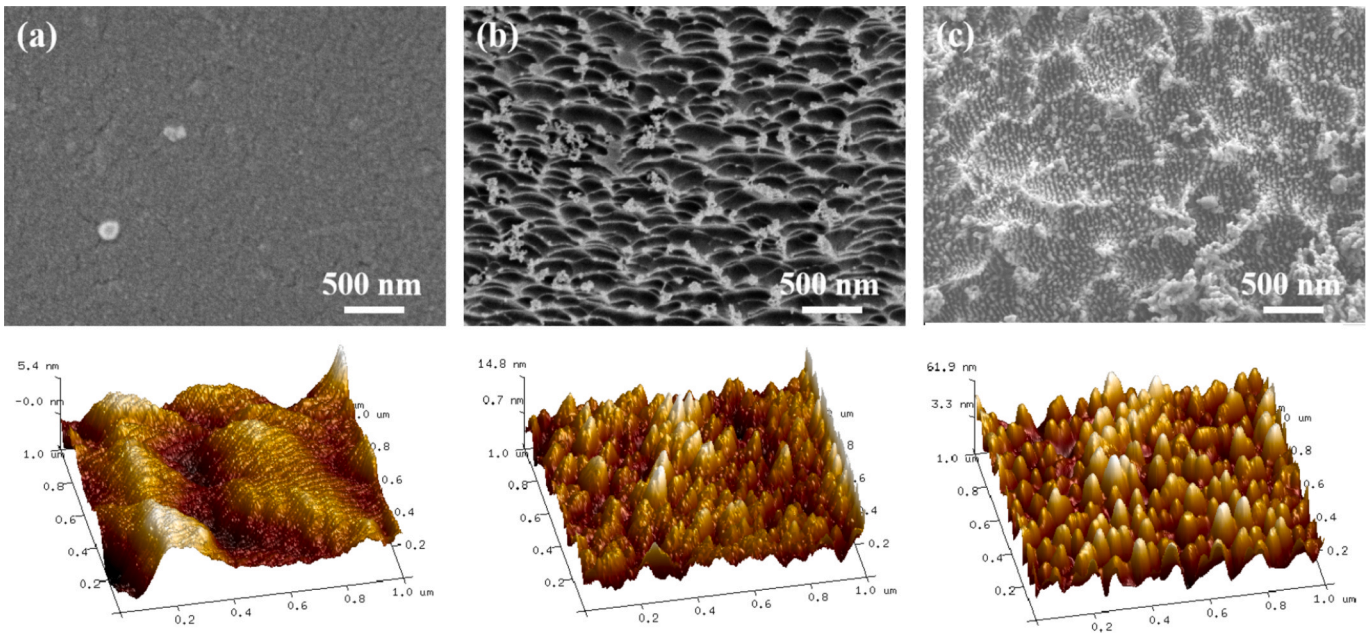

Fig. 2. Microstructures of polypropylene nonwoven fabrics with (a) untreatment, (b) 30 min etching, (c) 30 min etching and 20 s deposition.

where θ_{Wenzel} is the apparent contact angle, θ is the contact angle on an ideal smooth surface, and r is the roughness factor. An increase in the r amplifies the intrinsic wettability of a surface, rendering hydrophilic substrates more hydrophilic and hydrophobic substrates more hydrophobic. SEM images confirmed that surface roughness increased with longer oxygen plasma treatment. The observed superhydrophilicity could be attributed to this enhanced roughness coupled with the introduction of hydrophilic oxygen-containing groups by plasma. After complete wetting by water, the surface of the nonwoven fabrics was enveloped in a thick water layer, which prevented contact with oil droplets, thereby exhibiting oleophobic properties underwater [33].

To further verify the correlation between the hydrophilicity of the post-treatment nonwoven fabrics and surface functional groups, micro-infrared spectroscopy was employed to characterize the surface chemical composition alterations following different oxygen plasma treatments. As shown in Fig. S1 (supporting information), the original polypropylene nonwoven fabric is composed of hydrocarbon groups, with the carbon atoms exhibiting three bonding states: CH_2, CH_3, and C–H. After the first oxygen plasma etching, oxygen-containing functional groups such as OH, C=O, and C-O were introduced onto the surface of the nonwoven fabric. Following HMDSO deposition and subsequent oxygen plasma treatment for varying durations, the corresponding Micro-FTIR spectra were presented in Fig. 5. The peaks at 2850–2914 cm^{-1} and 2952 cm^{-1} correspond to the stretching vibrations of CH_2 and CH_3, confirming the preservation of hydrocarbon moieties [34,35]. Furthermore, the introduction of oxygen resulted in prominent O–H stretching vibrations at 3600–3100 cm^{-1} and C=O stretching vibrations at 1660 cm^{-1} [36,37]. The band at 1450 cm^{-1} was assigned to the bending vibrations of CH_X groups, while the characteristic $Si(CH_3)_X$ deformation vibration around 1270 cm^{-1} was not clearly distinguishable, likely due to overlap with the broad Si-O-Si vibrations in the 1200–950 cm^{-1} region [38]. In this range, absorptions corresponding to Si-O-Si (1070 cm^{-1}) and Si-C (1060 cm^{-1}) bonds were observed [39,40]. The peaks at 840 cm^{-1} and 802 cm^{-1} were attributed to Si-$(CH_3)_3$ and O-Si-$(CH_3)_2$, respectively [37]. These variations in absorption peaks could be elucidated by the complex structure of the polymethylsiloxane compounds.

XPS was employed to study the impact of varying plasma oxidation times on the elemental composition and chemical bonding states of nonwoven fabrics. Elemental composition was quantified via peak area calculations, yielding relative atomic percentages and silicon component analysis. The results were shown in Fig. 6b, and the calculation formulas were as follows:

$$\frac{n_i}{n_j} = \frac{I_i}{I_j} \times \frac{S_i}{S_j} \tag{2}$$

where n is the number of atoms, I is the intensity of the XPS peak (calculated as the peak area); S is the sensitivity factor. Fig. S2 (supporting information) presents the XPS survey spectra of polypropylene nonwoven fabrics before and after plasma etching. For the untreated sample, a pronounced C1s peak and a weak O1s peak were detected. After 30 min of plasma etching, the relative intensity of the C1s peak decreased, with its atomic percentage dropping from 91.6% to 86.0%, while the O1s peak significantly increased to 14.0% (Table S1, supporting information). After the HMDSO polymerization and deposition, the XPS spectrum of the sample exhibited C1s, O1s, and Si2p peaks, with carbon at 60.8%, oxygen at 21.7%, and silicon at 17.5%, resulting in a C/Si ratio of 3.47, consistent with HMDSO. Fig. 6a shows the XPS survey spectra of the fabric surface after the final oxygen plasma activation. The results indicated that all samples exhibited obvious C1s, O1s and Si2p peaks on the surface. The O/Si ratio of 1.23 was notably higher than the HMDSO with O/Si ratio of 0.5, which can be attributed to the oxygen plasma etching pre-treatment that introduced a large amount of oxygen-containing functional groups. After the secondary oxygen plasma treatment for varying durations, the relative intensity of the C1s peak decreased to 40.2%, while the O1s peak significantly increased to 41.7%, and the Si2p peak stabilized at 17.5 ± 0.6%. This observation indicated that as the prolonged oxygen plasma treatment time, oxygen ions break more carbon chains and introduce additional oxygen elements.

To further analyze the chemical bonding states, the C1s and Si 2p spectra were deconvoluted. Fig. 6c showed the C1s spectrum. Table 1 summarized the detailed fitting results for Polypropylene nonwoven fabrics with varying plasma oxidation time. Following oxygen etching pre-treatment, the C1s peaks of all samples could be decomposed into five distinct peaks: the C-Si peak (284.0 eV), the C–C peak (285.0 eV), the C-O peak (286.5 eV), the C=O peak (288.0 eV), and the O-C=O peak (289.1 eV) [41]. The relative contents of the oxidized carbon species (C=O and O-C=O) increased with plasma oxidation time (0–5 min), indicating that longer treatment introduced more oxygen atoms and

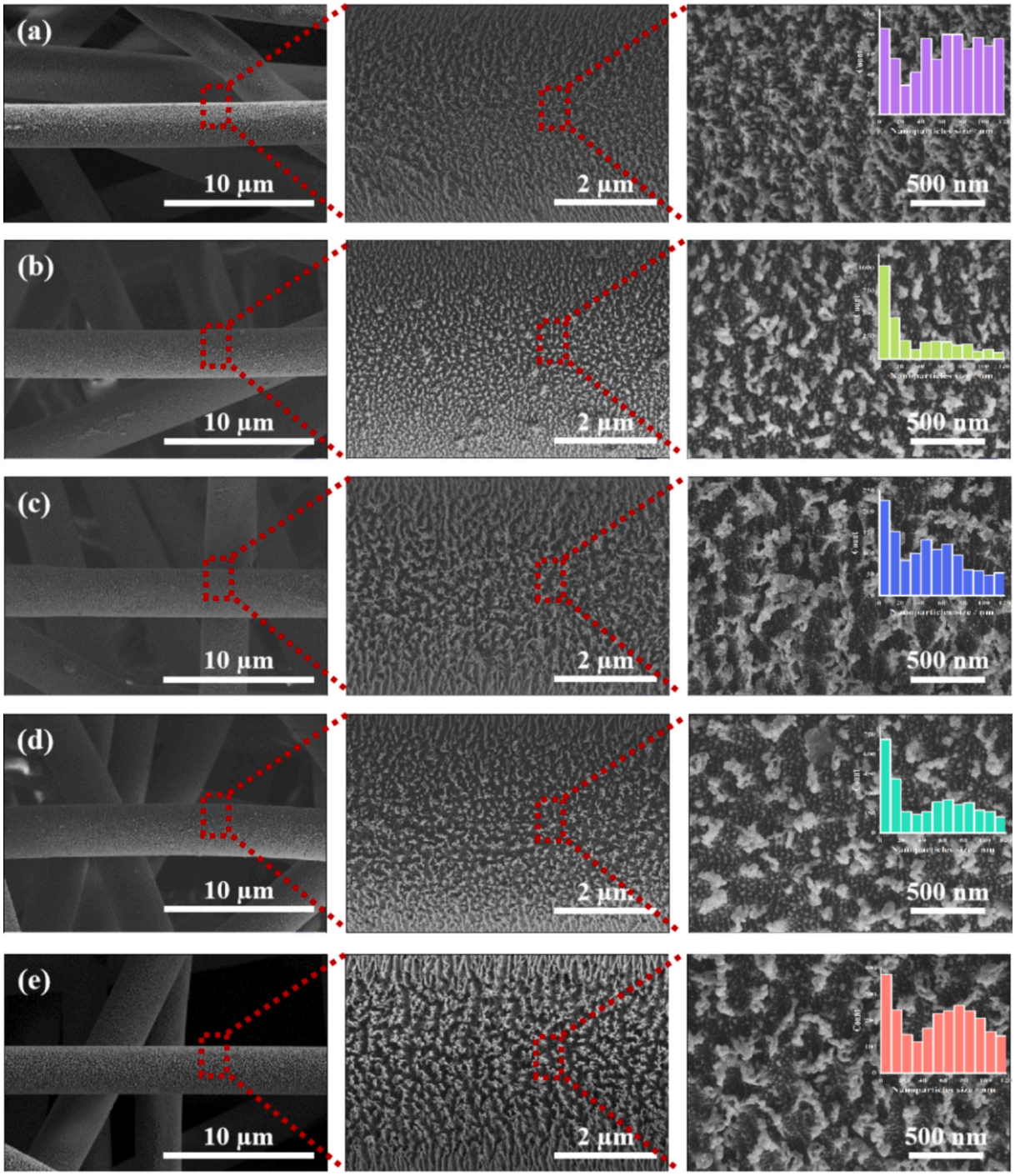

Fig. 3. SEM microstructures and nanoparticle size distribution of polypropylene nonwoven fabric treated with oxygen plasma for different times: (a) 1 min, (b) 2 min, (c) 3 min, (d) 4 min, and (e) 5 min. Scale bars correspond to magnification levels of 1000 X, 5000X, and 20,000X, respectively.

enhanced the surface oxidation degree. Conversely, the C-Si and C–C components remained relatively unchanged, suggesting the matrix structure was unaffected.

Fig. 6d showed the Si 2p spectrum. In films derived from HMDSO plasma polymerization, the Si 2p signal is typically deconvoluted into four components, Si-O$(CH_3)_3$, Si-$O_2(CH_3)_2$, Si-$O_3(CH_3)$, and Si-O_4, with binding energies of 101.5, 102.1, 102.8, and 103.4 eV, respectively, labeled as M, D, T, and Q. [42] The O/Si ratios were calculated from the following equations: [43]

$$O/Si = 0.5M + D + 1.5T + 2Q \quad (3)$$

where M, D, T and Q represent the area fractions of the individual components in Si2p. The results were statistically summarized in Table 1. The data in Table 1 revealed that one or two components dominate the Si 2p spectrum in each sample (each > 20%), which dictated the surface chemistry of the nonwoven fabrics. The M units were predominated in membrane structures deposited by HMDSO plasma, composed of −Si(CH_2)-Si$(CH_3)_2$-O-, −Si$(CH_2)_2$-Si$(CH_3)_2$-O- and −Si-Si$(CH_3)_2$-O-. The −O-Si$(CH_3)_2$-O- component, resulting from oxygen plasma etching pre-treatment, was the most abundant. In this process, the Si-CH_3 bonds were broken, allowing one silicon atom to connect to two oxygen atoms, forming a highly cross-linked polymer

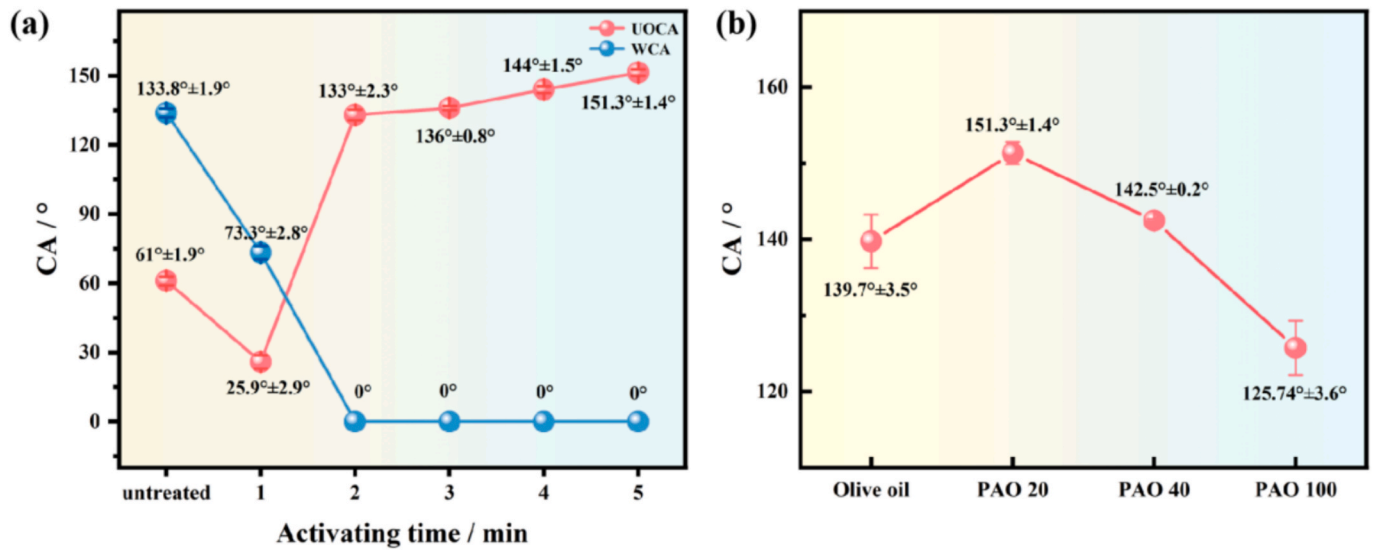

Fig. 4. (a) Variation of WCA and UOCA on the surface of polypropylene nonwoven fabrics after varying activating time; (b) different underwater oil contact angles.

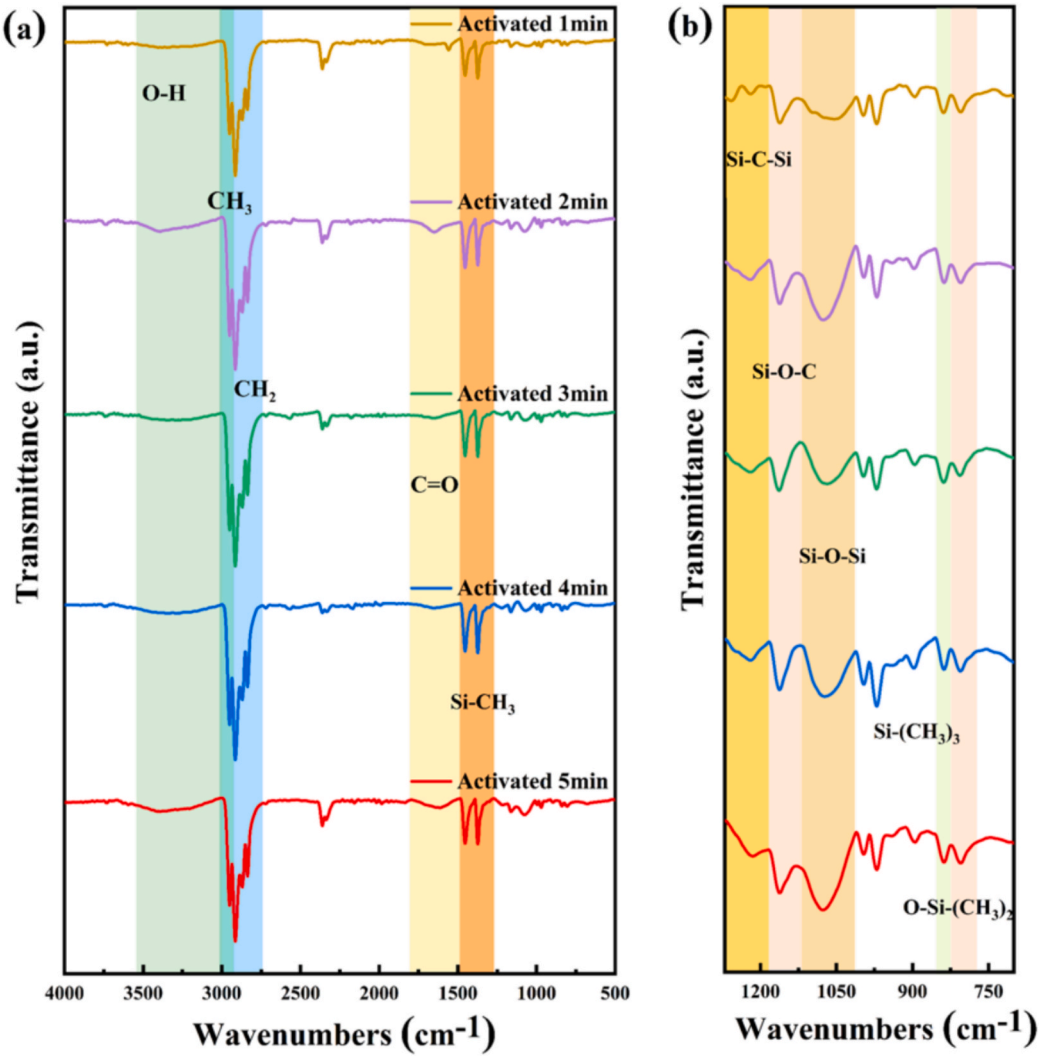

Fig. 5. Micro-FTIR spectra of polypropylene nonwoven fabrics after O_2 plasma treatment in the wavelength range of 4000 to 400 cm^{-1}.

network. Plasma oxidation induced the replacement of methyl groups in M, D, T, and Q with oxygen-containing groups or hydrogens, resulting in the formation of new conformations. A new component, $CH_2Si(CH_3)_3$, appeared in the fitted peak, which was labeled as S [44,45]. The

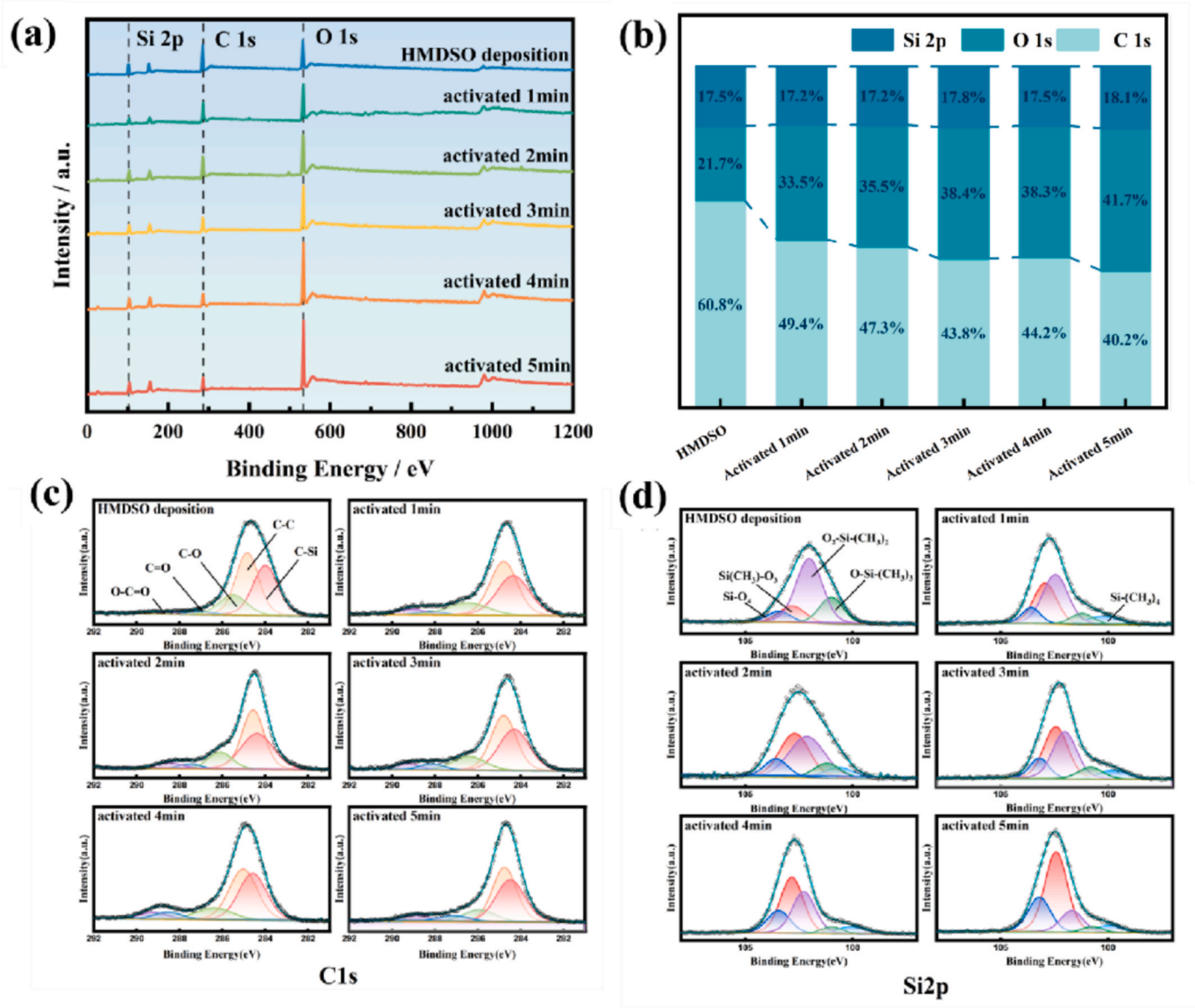

Fig. 6. XPS spectrum analysis of polypropylene nonwoven fabrics after O_2 plasma treatment; (a) full spectrum; (b) relative atomic percentage content; (c) C1s spectrum; (d) Si2p spectrum.

Table 1
Relative atomic percentage content of functional groups of C1s and Si2p before and after O_2 plasma treatment.

Sample	C1s					Si 2p				
	C-Si	C–C	C-O	C=O	O-C=O	S	M	D	T	Q
HMDSO	36.88	42.02	16.39	2.63	2.09	–	20.90	56.15	14.32	8.63
Activated 1 min	36.79	41.61	14.36	2.75	4.48	9.30	8.61	41.43	30.94	9.73
Activated 2 min	36.66	41.72	13.05	3.45	5.13	8.46	10.21	37.24	33.10	10.99
Activated 3 min	36.83	40.53	13.38	4.58	4.68	7.50	8.62	34.22	37.73	11.86
Activated 4 min	36.62	39.81	12.32	5.76	5.49	6.81	4.82	30.65	41.13	16.59
Activated 5 min	36.93	39.64	11.43	6.04	5.96	5.40	3.69	14.57	53.35	22.99

formation of S units may be attributed to the breakage of Si-O-Si chain segments and the introduction of carbon atoms due to high-intensity bombardment by the oxygen plasma. The $-O\text{-}Si(CH_3)_3$ component could also be attributed to this process. The total content of these non-oxidized components remained below 20% and progressively decreased with increasing the time of plasma oxidation, confirming that

longer treatment times promote oxidation. The D units decreased from 56.15% to 14.57% with increasing oxygen treatment time, while the T and Q component contents increased from 14.32% and 8.63% to 53.35% and 22.99%, respectively. This change suggested that increased plasma oxidation time led to a high degree of Si-C bond dissociation, resulting in greater bonding with oxygen atoms.

Combined FTIR and XPS analyses confirmed the presence of hydroxyl groups on samples after the secondary oxygen plasma treatment. The silicon oxide components in M, D, T, and Q possess two or more radical sites resulting in hydrophilic structures with terminal OH groups, such as $-O\text{-}Si(CH_3)_2\text{-}OH$, $-O_2\text{-}Si(CH_3)_2\text{-}OH$ and $-O\text{-}Si(OH)_3$, which explained the observed infrared spectral formation of complex branched and ringed networks. During the preparation process, the oxygen plasma initiated the methyl chains broken, generating free radicals and introducing oxygen elements. Subsequently, the HMDSO monomer broke down and polymerized to form a highly crosslinked polymer deposit layer. The oxygen plasma treatment further broke the methyl chains of the polymer layer, which then reacted with oxygen ions to form oxygen-containing functional groups, such as hydroxyl and carboxyl groups. This resulted in a stable, cross-linked siloxane matrix on the fiber surface, wherein the originally hydrophobic methyl groups were progressively replaced by hydrophilic moieties as treatment time increased. Moreover, the etching effect of the oxygen plasma, combined with the varying sizes of nanoparticles obtained from HMDSO deposition, significantly enhanced the roughness of the fiber surface. Ultimately, the synergistic combination of this hydrophilic surface chemistry and the hierarchical roughness imparted durable superhydrophilicity to the nonwoven fabrics.

To evaluate the performance stability, cyclic oil–water separation tests were conducted, as illustrated in Figs. 7a and 7b. The oil–water mixture was prepared by combining the 20 mL dyed PAO oil with 40 mL of deionized water. Pre-wetted modified nonwoven fabrics were positioned in the separation device, and the separated water was collected in a conical flask. The separation efficiency was calculated using Equation (4) [46]:

$$E = \frac{m_1}{m_0} \times 100\% \tag{4}$$

where E is the oil–water separation efficiency, m_0 is the mass of oil before the separation test, and m_1 is the mass of oil after the separation test. After the separation, PAO oil was effectively trapped, while water flowed completely into the conical flask with no residual oil observed. In contrast, the untreated PP fabric failed to separate the mixture. As shown in Fig. S3, the pristine fabric was rapidly wetted and penetrated by the oil, allowing it to pass through. This control experiment confirmed the necessity of surface modification for effective separation. Table 2 presented a comparison of the cyclic oil–water separation efficiencies of fabric materials subjected to different surface hydrophilic modifications. Oil residue was observed on the modified nonwoven fabrics after 35 cycles. However, as shown in Fig. 7b, rinsing with water could remove oil droplets quickly, leaving no traces of contamination, which demonstrated excellent self-cleaning properties. Furthermore, the separation efficiency consistently remained above 99.0%, showing outstanding recycling performance compared to other modification methods. The chemical stability tests were conducted by immersing the modified samples in acidic (pH = 1, 5), alkaline (pH = 9, 13), and saline (3.5 wt% NaCl) solutions for 24 h, as detailed in Fig. 7d. Aqueous solutions with pH values of 1, 5, 9, 13, and a 3.5 wt% NaCl solution were prepared using HCl, NaOH, and NaCl. The samples modified by 5 min of plasma oxidation were immersed in these solutions for 24 h. The results indicated that the modified nonwoven fabrics remained directly wettable by water after soaking in various solutions, retaining their superhydrophilicity. SEM images (Fig. S4, Supporting Information) revealed that while the surface nanostructure was somewhat altered, nanoparticle clusters remained evenly distributed, and the overall morphology was largely retained [47,48]. The observation confirmed the exceptional resistance to acidic, alkaline and saline corrosive environments even after prolonged exposure, demonstrating excellent chemical stability facilitated effective separation of complex oil–water mixtures.

To assess the impact of different plasma oxidation time on the aging properties of the samples, water contact angle measurements were taken every five days. The results were illustrated in the Fig. 7e. The 1 min plasma-oxidized sample exhibited an increase in contact angle to 125° after one day exposed to air, showing hydrophobicity. Samples subjected to 2–5 min of plasma oxidation maintained superhydrophilicity for 260 days, with varying imbibition rates. Longer plasma oxidation time correlated with faster imbibition. The fabrics treated for 5 min exhibited imbibition within 10 s, whereas those treated for 2–4 min required over 1 min for complete wetting. This remarkable long-term stability originates from the unique surface architecture constructed by the synergistic combination of HMDSO deposition and subsequent O_2 plasma treatment. The key lies in the fact that HMDSO first forms a highly cross-linked siloxane polymer network on the fiber surface. This network serves as a robust matrix that not only suppresses the migration and rotation of polypropylene polymer chains but, more fundamentally, provides a stable, non-aging platform resistant to physical aging and chemical degradation. The subsequent O_2 plasma treatment does not merely attach hydrophilic groups superficially. Rather, it cleaves the $-CH_3$ groups on the siloxane network and replaces them in situ with strongly hydrophilic, hydrogen-bond-capable functionalities such as –OH and –COOH groups. These hydrophilic moieties are covalently anchored to the cross-linked backbone, thereby being “permanently locked” within this rigid, non-aging matrix. This architecture explicitly addresses and mitigates the plasma aging effect by avoiding the loss of hydrophilicity typically caused by surface energy relaxation or functional group reorientation in conventional plasma treatments [49].

To elucidate the mechanism of oil–water separation, capillary phenomena on the superhydrophilic and underwater superoleophobic polypropylene nonwoven fabrics surface were analyzed. Capillary phenomena, illustrated in Fig. 7f, referred to the rise (in wetting liquids) or fall (in non-wetting liquids) of a liquid within narrow tubes or porous materials.[50] The capillary phenomenon in fabric materials required the introduction of the concept of a capillary force difference (ΔP), which can be derived from the following equation: [51,52]

$$\Delta P = \frac{2\gamma\cos\theta}{R} \tag{5}$$

where ΔP represents the capillary pressure force difference, γ is the liquid's surface tension, cos θ is the contact angle of water or oil with the

Table 2
Oil/water separation properties of fabric materials after different surface hydrophilic treatments.

Substrate	Treated method	Oil	Cycle times	Efficiency	References
Cotton fabrics	Dip-coated	N-octane	25	99.3	[8]
Cotton fabrics	Dip-coated	Dichloromethane	25	98	[53]
Cotton fabrics	Scrape-coating	Motor oil	30	97.5	[54]
Polyamide nonwoven fabrics	Coating with pre-etching	Heavy mineral oil	25	98.6	[55]
Polypropylene nonwoven fabrics	Plasma polymerization + plasma oxidation	PAO	35	99.0	Our work

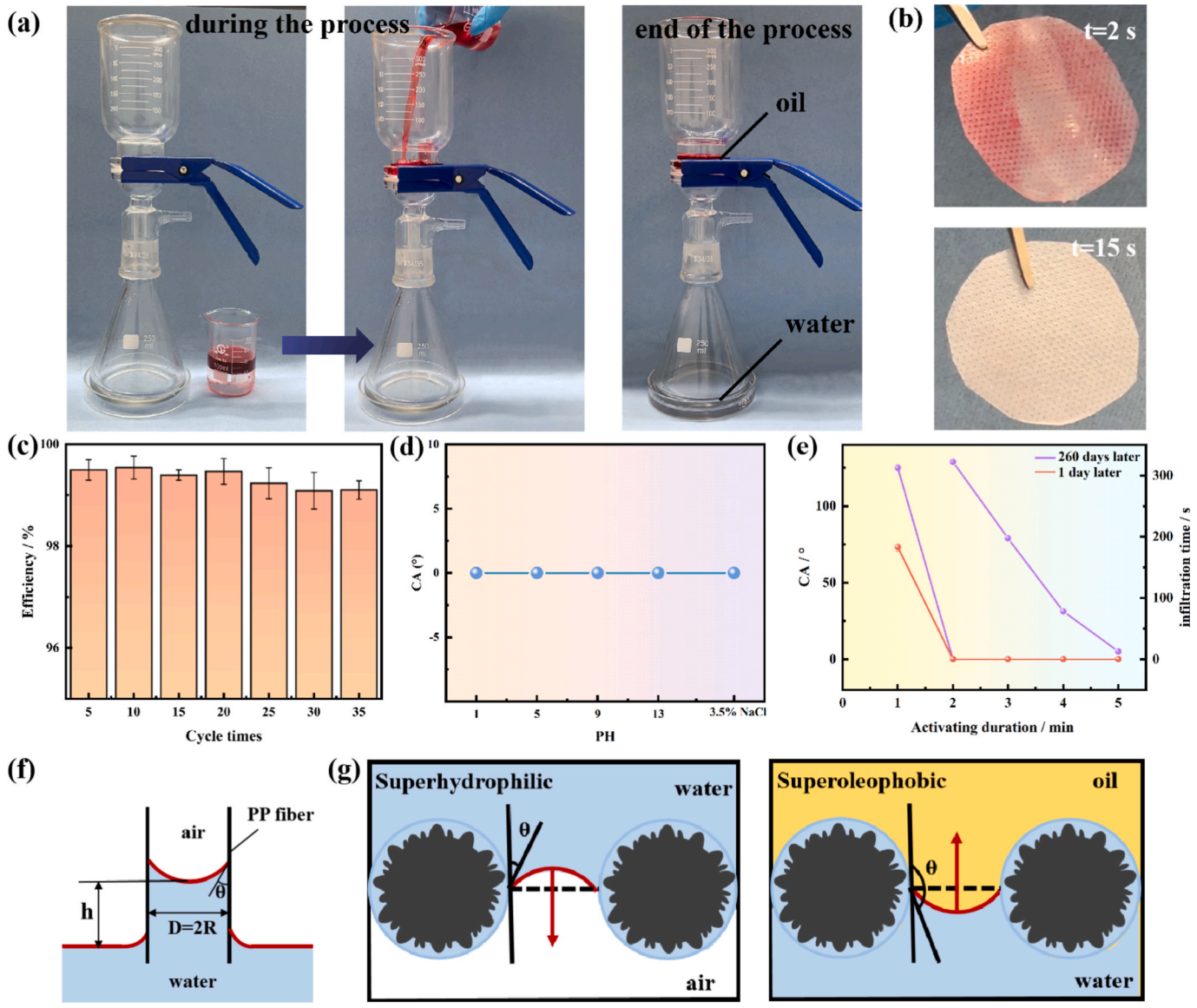

Fig. 7. Performance and mechanism of the modified PP nonwoven fabric. (a) Schematic of the cyclic oil–water separation experiment; (b) self-cleaning demonstration via water rinsing; (c) oil–water separation efficiency over multiple cycles; (d) chemical stability evaluated by water contact angles after immersion in solutions of varying pH and salinity; (e) long-term stability: water contact angle versus aging time in air; (f) schematic of capillary action explaining the separation mechanism; (g) the mechanism of oil–water separation.

fabric surface, and R is the theoretical radius of the fabric's capillaries. The gravitational force (G) generated by the liquid level height difference can be expressed by equation (6).

$$G = \rho g h \tag{6}$$

In the equation, ρ represents density, g is the acceleration due to gravity, and h denotes the height difference, either the rise or fall of a liquid, induced by an internal and external pressure difference, ΔP. When ΔP is in equilibrium with G, h can be expressed as shown in equation (7):

$$h = \frac{2\gamma\cos\theta}{\rho g R} \tag{7}$$

Polypropylene nonwoven fabrics were composed of intersecting fibers, with interstitial spaces between adjacent fibers ranging from 30-100 μm, functioning as capillary channels (with an inner diameter equal to or less than 1 mm). According to equation (5), when $0 < \theta < 90^{\circ}$, $\Delta P > 0$, the capillary pressure force difference facilitates liquid penetration into the capillary; conversely, when $\theta > 90^{\circ}$, $\Delta P < 0$, the capillary pressure force difference impedes liquid entry into the capillary. For superhydrophilic polypropylene nonwoven fabrics, the combined capillary pressure and gravity effects facilitated rapid wetting upon water droplet contact. The water rise height (h_W) within the capillaries can be derived from equation (7). Considering $\theta = 0^{\circ}$, $\cos\theta = 1$, $\gamma_{WA} = 0.073 N m^{-1}$, $\rho = 1.0 \times 10^3\, kg m^{-3}$, $g = 9.8\, m s^{-2}$, $R = 3.0 - 10.0 \times 10^{-5}$ m, the calculated $h_W = 0.15 - 0.50$m m. This result indicated that the capillary rise of water substantially surpassed the thickness of the polypropylene nonwoven fabrics (approximately 1 mm).

For underwater superoleophobic polypropylene nonwoven fabrics, oil droplets were repelled upon contact with the aqueous environment, remaining external to the water layer. The oil rise height (h_O) on the surface of underwater superoleophobic nonwoven fabrics can be derived via equation (7). By setting $\theta = 180^{\circ}$, $\cos\theta = -1$, the interfacial tension between oil and water $\gamma_{OW} = 0.03 N m^{-1}$, oil density $\rho_O = 0.5 \times 10^3\, kg m^{-3}$, R=R $= 6.5 \times 10^{-5}$ m, $h_O = -0.19$m. The negative value for the oil rise height indicated that the oil droplet, under its own weight, overcame capillary pressure and reached the fabrics surface only when

the oil layer height reached 0.19 m. Furthermore, buoyancy from the water further influences oil droplets. Consequently, oil droplets suspended on the water film are prevented from penetrating the nonwoven fabric due to capillary forces, resulting in interception outside the water film. The results of the oil–water separation tests confirmed this observation.

After plasma modification, the fabric exhibits persistent hydrophilicity at the chemical level. At the same time, a multi-scale capillary network is formed through combined etching and deposition, which adds nanoscale roughness to the original micron-scale fiber gaps. These micro-nano structures collectively enhance capillary forces and Laplace pressure. As a result, rapid water transport and stable underwater superoleophobicity are achieved, enabling efficient and durable oil–-water separation. Extensive research has shown that conventional single-step plasma treatments can initially impart hydrophilicity to polymer surfaces, but the modified effects often rapidly diminish due to the relaxation of polymer chains and the rearrangement of functional groups. Hydrophilicity typically decreases significantly within days to weeks [8,20,21]. Even with optimized radio-frequency plasma treatments, the stability period of hydrophilicity generally remains on the order of a hundred days [56–59]. In contrast to these studies, our method employs a three-step synergistic strategy of 'oxygen plasma etching-HMDSO deposition-secondary oxygen plasma activation' to construct a highly cross-linked siloxane network on the PP fiber surface. This network not only covalently anchors hydrophilic functional groups such as hydroxyl and carboxyl groups but also provides a rigid matrix that suppresses polymer chain migration, thereby synergistically inhibiting the aging process from both physical and chemical perspectives.

4. Conclusion

In this study, polypropylene nonwoven fabrics were modified via a PECVD strategy comprising oxygen plasma etching pre-treatment, HMDSO deposition, and subsequent oxygen plasma treatment. By varying the treatment time, the superhydrophilic and underwater superoleophobic polypropylene nonwoven fabrics were obtained. The distinct reactivities of the crystalline and amorphous regions of polypropylene nonwoven fabrics toward oxygen ions facilitated the formation of a bionic fish scale-like surface roughness. The micro-nano structure was achieved through the pre-treatment process, while the subsequent HMDSO deposition introduced nanoparticles of varying sizes through oxygen ion treatment, significantly increasing the surface roughness of the fibers. Additionally, the degree of crosslinking on the fabrics surface was enhanced, leading to the introduction of hydrophilic functional groups, such as hydroxyl and carboxyl groups. These modifications resulted in an extremely low water contact angle (achieving a wetting state), and an exceptionally high underwater oil contact angle (reaching 151°). The modified fabrics exhibited exceptional long-term environmental durability, maintaining superhydrophilicity for over 260 days without performance decay. This solvent-free, energy-efficient platform overcame traditional modification limitations, offering a scalable solution for oil pollution treatment.

CRediT authorship contribution statement

Xueqing Zhao: Writing – original draft, Investigation, Data curation. **Changying Chen:** Software, Investigation, Data curation. **Guanshui Ma:** Writing – review & editing, Supervision. **Peng Guo:** Writing – review & editing, Methodology. **Rende Chen:** Supervision. **Peiling Ke:** Funding acquisition. **Aiying Wang:** Writing – review & editing, Supervision, Funding acquisition, Conceptualization.

Declaration of competing interest

The authors declare that they have no known competing financial interests or personal relationships that could have appeared to influence the work reported in this paper.

Acknowledgements

Xueqing Zhao and Changying Chen contributed equally to this work. This work was financially supported by the National Natural Science Foundation of China (U24A2030), and the Natural Science Foundation of Ningbo (2023Z110).

Appendix A. Supplementary data

Supplementary data to this article can be found online at https://doi.org/10.1016/j.apsusc.2026.166656.

Data availability

Data will be made available on request.

References

[1] A. Saravanan, P. Kumar, K. Vardhan, S. Jeevanantham, S. Karishma, P. Yaashikaa, P. Vellaichamy, A review on systematic approach for microbial enhanced oil recovery technologies: Opportunities and challenges, J. Clean. Prod. 258 (2020) e12077, https://doi.org/10.1016/j.jclepro.2020.120777.
[2] D. Salam, M. Suidan, A. Venosa, Biodegradation and toxicity of vegetable oils in contaminated aquatic environments: effect of antioxidants and oil composition, Sci. Total Environ. 547 (2016) 95–103, https://doi.org/10.1016/j.scitotenv.2015.12.138.
[3] S. Fu, H. Zhou, H. Wang, H. Niu, W. Yang, H. Shao, J. Wang, T. Lin, Superhydrophilic, underwater directional oil-transport fabrics with a novel oil trapping function, ACS Appl. Mater. Interfaces 11 (30) (2019) 27402–27409, https://doi.org/10.1021/acsami.9b06533.
[4] M. Long, S. Peng, W. Deng, N. Wen, Q. Zhou, W. Deng, Oil/Water Separations from nanosized superhydrophobic to microsized under-oil superhydrophilic dust, ACS Appl. Nano Mater. 1 (7) (2018) 3398–3406, https://doi.org/10.1021/acsanm.8b00615.
[5] N. Suvindran, F. Li, Y. Pan, X. Zhao, Characterization and bioreplication of tradescantia pallida inspired biomimetic superwettability for dual way patterned water harvesting, Adv. Mater. Interfaces 5 (19) (2018) 1800723, https://doi.org/10.1002/admi.201800723.
[6] K. Jiang, Z. Yang, Y. Luo, X. Xue, F. Li, B. Bhushan, Y. Pan, Y. Huo, X. Zhao, L. Li, J. Wei, W. Cao, Seaweed-inspired underwater anti-oil-fouling and anti-fogging coating with mechanical durability, J. Colloid Interface Sci. 664 (2024) 801–808, https://doi.org/10.1016/j.jcis.2024.02.206.
[7] B. Cortese, D. Caschera, G. Padeletti, G. Ingo, G. Gigli, A brief review of surface-functionalized cotton fabrics, Surf. Innov. 1 (3) (2013) 140–156, https://doi.org/10.1680/si.13.00008.
[8] P. Yang, J. Yang, Z. Wu, X. Zhang, Y. Liu, M. Lu, Facile fabrication of superhydrophilic and underwater superoleophobic surfaces on cotton fabrics for effective oil/water separation with excellent anti-contamination ability, Colloids Surf A Physicochem Eng Asp 628 (2021) e127290, https://doi.org/10.1016/j.colsurfa.2021.127290.
[9] Y. Lee, Y. Park, O. Kwon, S. Kim, S. Chung, M. Moon, Hygroscopic ramie fabrics for recovering highly viscous low sulfur fuel oil, Environ. Pollut. 308 (2022) e119668, https://doi.org/10.1016/j.envpol.2022.119668.
[10] H. Zhang, Z. Guo, A superhydrophilic and robust fabric, featuring self-assembled layers of chitosan and carbon nanotubes, facilitates high-throughput oil-water separation, Sep. Purif. Technol. 344 (2024) e127233, https://doi.org/10.1016/j.seppur.2024.127233.
[11] H. Wang, X. Wang, Y. Yu, B.B. Mamba, X. Jiang, X. Yang, L. Shao, Engineering self-rebound catalytic membranes for efficient high-viscosity oily wastewater purification and emerging contaminants removal, Water Res. 288 (2026) 124750, https://doi.org/10.1016/j.watres.2025.124750.
[12] S. Gao, F. Zhang, J. Jin, Nature-inspired superwetting membranes for emulsified oily water separation, ACS Nano 19 (12) (2025) 11489–11500, https://doi.org/10.1021/acsnano.5c01252.
[13] N. Zhang, J. Zhang, X. Yang, C. Zhou, X. Zhu, B. Liu, Y. Chen, S. Lin, Z. Wang, Janus membrane with hydrogel-like coating for robust fouling and wetting resistance in membrane distillation, ACS Appl. Mater. Interfaces 15 (15) (2023) 19504–19513, https://doi.org/10.1021/acsami.3c02781.
[14] X. Wang, K. Zhao, W. Cao, D. Ji, Z. Ye, Z. Su, G. Gao, Z. Wang, C. Sun, Y. Liu, L. Zhang, T. Zhang, F. Li, J. Zhu, Polyimide-Coating-on-Aramid nanofiber strategy toward ultralight organic aerogels with multifunctional properties, Chem. Eng. J. 499 (2024) 155939, https://doi.org/10.1016/j.cej.2024.155939.
[15] J. Allen, The plasma-sheath boundary: its history and Langmuir's definition of the sheath edge, Plasma Sources Sci. Technol. 18 (1) (2009) e14004, https://doi.org/10.1088/0963-0252/18/1/014004.
[16] S. Ahmed, G. Rho, J.Y. Lee, S. Kim, H. Kim, J. Yong, M. Moon, K. Lee, Nano-embossed structure on polypropylene induced by low energy Ar ion beam

irradiation, Surf. Coat. Tech. 205 (2010) 104–108, https://doi.org/10.1016/j.surfcoat.2010.06.005.
[17] T. Ko, S. Cho, S. Kim, Y. Lee, D. Kim, W. Jo, H. Kim, S. Yang, K. Oh, M. Moon, Direct recovery of spilled oil using hierarchically porous oil scoop with capillary-induced anti-oil-fouling, J. Hazard. Mater. 410 (2020) 124549, https://doi.org/10.1016/j.jhazmat.2020.124549.
[18] M. Asai, D. Zhao, S. Kumar, Role of grafting mechanism on the polymer coverage and self-assembly of hairy nanoparticles, ACS Nano 11 (7) (2017) 7028–7035, https://doi.org/10.1021/acsnano.7b02657.
[19] Y. Park, N. Inagaki, Surface modification of poly (vinylidene fluoride) film by remote Ar, H_2, and O_2 plasmas, Polymer 44 (5) (2003) 1569–1575, https://doi.org/10.1016/S0032-3861(02)00872-8.
[20] R. Morent, N. Geyter, L. Gengembre, C. Leys, E. Payen, Study of the ageing behaviour of polymer films treated with a dielectric barrier discharge in air, helium and argon at medium pressure, Surf. Coat. Tech. 201 (18) (2007) 7847–7854, https://doi.org/10.1016/j.surfcoat.2007.03.018.
[21] M. Pascual, R. Balart, L. Sánchez, O. Fenollar, O. Calvo, Study of the aging process of corona discharge plasma effects on low density polyethylene film surface, J. Mater. Sci. 43 (2008) 4901–4909, https://doi.org/10.1007/s10853-008-2712-0.
[22] H. Dirk, B. Ezgi, H. Barbara, S. Urs, A. Martin, G. Sandra, Plasma polymerization of hexamethyldisiloxane: Revisited, Plasma Process. Polym. 18 (2) (2020) e2000176, https://doi.org/10.1002/ppap.202000176.
[23] C. Nwankire, G. Favaro, Q. Duong, D. Dowling, Enhancing the mechanical properties of superhydrophobic atmospheric pressure plasma deposited siloxane coatings, Plasma Process. Polym. 8 (4) (2011) 305–315, https://doi.org/10.1002/ppap.201000069.
[24] A. Freitas, C. Maciel, J. Rodrigues, R. Ribeiro, S. Delgado, E. Rangel, Organosilicon films deposited in low-pressure plasma from hexamethyldisiloxane-a review, Vacuum 194 (2021) e110556, https://doi.org/10.1016/j.vacuum.2021.110556.
[25] F. Palumbo, C. Lo Porto, P. Favia, Plasma Nano-Texturing of Polymers for Wettability Control: Why, What and How, Coatings, 9(10) (2019) 640, 10.3390/coatings9100640.
[26] R.D. Mundo, R. d'Agostino, F. Palumbo, Long-lasting antifog plasma modification of transparent plastics, ACS Appl. Mater. Interfaces 6 (19) (2014) 17059–17066, https://doi.org/10.1021/am504668s.
[27] F. Palumbo, R.D. Mundo, D. Cappelluti, R. d'Agostino, SuperHydrophobic and superhydrophilic polycarbonate by tailoring chemistry and nano-texture with plasma processing, Plasma Process. Polym. 8 (2) (2011) 118–126, https://doi.org/10.1002/ppap.201000098.
[28] M. Saget, N. Nuns, P. Supiot, C. Foissac, S. Bellayer, K. Dourgaparsad, P. Royoux, G. Delaplace, V. Thomy, Y. Coffinier, M. Jimenez, Ultra-hydrophobic biomimetic transparent bilayer thin film deposited by atmospheric pressure plasma, Surf. Interf 42 (2023) e103398, https://doi.org/10.1016/j.surfin.2023.103398.
[29] E. Wohlfart, J. Fernández-Blázquez, E. Knoche, A. Bello, E. Pérez, E.A. Arzt, Campo Nanofibrillar patterns by Plasma Etching: the influence of polymer crystallinity and orientation in surface morphology, Macromolecules 43 (2020) 9908–9917, https://doi.org/10.1021/ma101889s.
[30] M. Pedroni, E. Vassallo, M. Aloisio, A. Brasca, H. Chen, R. Donnini, G. Firpo, S. Morandi, S. Pietralunga, T. Silvetti, G. Speranza, T. Virgili, Nature-inspired antibacterial poly (butylene succinate) (PBS) by plasma etching nanotexturing for food packaging applications, Surf. Coat. Tech. 471 (2023) e129828, https://doi.org/10.1016/j.surfcoat.2023.129828.
[31] C. Roth, G. Oberbossel, E. Buitrago, R. Heuberger, P. Rohr, Nanoparticle synthesis and growth in a continuous plasma reactor from organosilicon precursors, Plasma Process. Polym. 9 (2) (2012) 119–134, https://doi.org/10.1002/ppap.201100180.
[32] R. Wenzel, Resistance of solid surfaces to wetting by water, Ind. Eng. Chem. 28 (1936) 988–994, https://doi.org/10.1021/ie50320a024.
[33] Y. Tian, B. Su, L. Jiang, Interfacial material system exhibiting superwettability, Adv. Mater. 26 (40) (2014) 6872–6897, https://doi.org/10.1002/adma.201400883.
[34] B. Smith, The infrared spectra of polymers III: hydrocarbon polymers, Spectroscopy, 36 (11) (2021) 22-25, 10.56530/spectroscopy.mh7872q7.
[35] A. Gopanna, R. Mandapati, S.P. Thomas, K. Rajan, M. Chavali, Fourier transform infrared spectroscopy (FTIR), Raman spectroscopy and wide-angle X-ray scattering (WAXS) of polypropylene (PP)/cyclic olefin copolymer (COC) blends for qualitative and quantitative analysis, Polym. Bull. 76 (8) (2019) 4259–4274, https://doi.org/10.1007/s00289-018-2599-0.
[36] E. Noemi, V. Vikrant, G. Thomas, D. Hegemann, M. Heuberger, Response of Plasma-polymerized hexamethyldisiloxane films to aqueous environments, Langmuir 31 (47) (2015) 12944–12953, https://doi.org/10.1021/acs.langmuir.5b03010.
[37] J. Bour, J. Bardon, H. Aubriet, D. Frari, B. Verheyde, R. Dams, D. Vangeneugden, D. Ruch, Different ways to plasma-polymerize HMDSO in DBD configuration at atmospheric pressure for corrosion protection, Plasma Process. Polym. 5 (8) (2008) 788–796, https://doi.org/10.1002/ppap.200800052.
[38] R. Morent, N. Geyter, T. Jacobs, S. Vlierberghe, P. Dubruel, C. Leys, E. Schacht, Plasma-polymerization of HMDSO using an atmospheric pressure dielectric barrier discharge, Plasma Process. Polym. 6 (1) (2009) s537–s542, https://doi.org/10.1002/ppap.200931101.
[39] R. Gandhiraman, S. Daniels, D.C. Cameron, B. McNamara, E. Tully, R. O'Kennedy, PECVD of biocompatible coatings on 316L stainless steel, Surf. Coat. Tech. 200 (1–4) (2005) 1031–1035, https://doi.org/10.1016/j.surfcoat.2005.02.009.
[40] V. Purohit, E. Mielczarski, J. Mielczarski, L. Akesso, Evidence of coexistence of micro and nanoporosity of organo-silica polymeric films deposited on silicon by plasma deposition, Mater. Chem. Phys. 141 (2–3) (2013) 602–612, https://doi.org/10.1016/j.matchemphys.2013.04.040.
[41] C. Ma, L. Wang, A. Nikiforov, Y. Onyshchenko, P. Cools, K. Ostrikov, N. Geyter, R. Morent, Atmospheric-pressure plasma assisted engineering of polymer surfaces: from high hydrophobicity to superhydrophilicity, Appl. Surf. Sci. 535 (2020) e147032, https://doi.org/10.1016/j.apsusc.2020.147032.
[42] R. Maurau, N. Boscher, J. Guillot, P. Choquet, Nitrogen introduction in pp-HMDSO thin films deposited by atmospheric pressure dielectric barrier discharge: an XPS Study, Plasma Process. Polym. 9 (3) (2012) 316–323, https://doi.org/10.1002/ppap.201100144.
[43] L. O'Hare, A. Hynes, R. Alexander, A methodology for curve-fitting of the XPS Si 2p core level from thin siloxane coatings, Surf. Interface Anal. 39 (2007) 926–936, https://doi.org/10.1002/sia.2634.
[44] G. Dakroub, T. Duguet, J. Esvan, C. Lacaze-Dufaure, S. Roualdes, V. Rouessac, Comparative study of bulk and surface compositions of plasma polymerized organosilicon thin films, Surf. Interf. 25 (2021) e101256, https://doi.org/10.1016/j.surfin.2021.101256.
[45] S. Yoshimura, S. Sugimoto, K. Murai, M. Kiuchi, Low-energy mass-selected ion beam production of fragments produced from hexamethyldisiloxane for the formation of silicon oxide film, Surf. Coat. Techn. 313 (2017) 402–406, https://doi.org/10.1016/j.surfcoat.2017.02.009.
[46] J. Song, Q. Yu, X. Liang, Q. Rao, P. Wang, M. Lu, H. Xiao, Micro-dissolved fabrication of robust superhydrophilic and underwater superoleophobic membranes based on cotton fabrics for oil/water separation, Cellul. 30 (2) (2022) 1073–1086, https://doi.org/10.1007/s10570-022-04890-2.
[47] J. Kim, M. Moon, H. Kim, Capillary rise in superhydrophilic rough channels, Phys. Fluids 32 (3) (2020) e032105, https://doi.org/10.1063/1.5133826.
[48] Y. Lee, S. Cho, S. Choi, O. Kwon, S. Yoon, S. Kim, K. Park, S. Chung, M. Moon, Slippery, Water-infused membrane with grooved nanotrichomes for lubricating-induced oil repellency, Adv. Sci. 9 (13) (2022) e2103950, https://doi.org/10.1002/advs.202103950.
[49] T. Egghe, R. Ghobeira, R. Morent, R. Hoogenboom, N. Geyter, Comparative study of the aging behavior of plasma activated hexamethyldisiloxane-based plasma polymers and silicone elastomer thin films, Prog. Org. Coat. 172 (2022) 107091, https://doi.org/10.1016/j.porgcoat.2022.107091.
[50] N. Morrow, G. Mason, Recovery of oil by spontaneous imbibition, Curr. Opin. Colloid Interface Sci. 6 (4) (2001) 321–337, https://doi.org/10.1016/S1359-0294(01)00100-5.
[51] Z. Zhang, J. Wei, X. Zhang, H. Xiao, Y. Liu, M. Lu, Polyester fabrics coated with cupric hydroxide and cellulose for the treatment of kitchen oily wastewater, Chemosphere 302 (2022) 134840, https://doi.org/10.1016/j.chemosphere.2022.134840.
[52] H. Zhou, H Wang., H. Niu, T. Lin, Superphobicity/philicity Janus fabrics with switchable, spontaneous, directional transport ability to water and oil fluids, Sci. Rep. 3 (2013) 2964, 10.1038/srep02964.
[53] T. Yan, X. Chen, T. Zhang, J. Yu, X. Jiang, W. Hu, F. Jiao, A magnetic pH-induced textile fabric with switchable wettability for intelligent oil/water separation, Chem. Eng. J. 347 (2018) 52–63, https://doi.org/10.1016/j.cej.2018.04.021.
[54] S. Yang, M. Li, G. Fang, M. Xue, Y. Lu, Flexible cement-sand coated cotton fabrics with superhydrophilic and underwater superoleophobic wettability for the separation of water/oil mixtures and oil-in-water emulsions, Colloid Surf. Physicochem. Eng. Asp. 608 (2020) e25611, https://doi.org/10.1016/j.colsurfa.2020.125611.
[55] P. Zhao, N. Qin, C. Ren, J. Wen, Surface modification of polyamide meshes and nonwoven fabrics by plasma etching and a PDA/cellulose coating for oil/water separation, Appl. Surf. Sci. 481 (2019) 883–891, https://doi.org/10.1016/j.apsusc.2019.03.152.
[56] D. Pal, S. Neogi, S. De, Comparative study of hydrophilic modification of polyacrylonitrile membranes by nitrogen and carbon dioxide RF plasma, Polym. Eng. Sci. 59 (10) (2019) 2148–2158, https://doi.org/10.1002/pen.25217.
[57] D. Pal, S. Neogi, S. De, Hydrophilic surface modification of polyacrylonitrile based membrane: effect of low temperature radio frequency carbon dioxide plasma, Polym. Bull. 75 (2018) 3567–3586, https://doi.org/10.1007/s00289-017-2230-9.
[58] M. Li, Z. Zhao, M. Wang, Controllable modification of polymer membranes by LDDLT plasma flow: membrane module scale-up and hydrophilic stability, Chem. Eng. Sci. 122 (2015) 53–63, https://doi.org/10.1016/j.ces.2014.09.015.
[59] T.T.A. Owad, E.A.A. Siddig, R.E.M. Salih, Y. Zhang, C. Wang, Y. Xu, J. Zhang, Durable and recoverable hydrophilicity of polyethylene terephthalate fabric prepared with plasma selective etching, Surf. Interf. 32 (2022) 102081, https://doi.org/10.1016/j.surfin.2022.102081.